

Infrared microspectroscopic studies on the pitting of AA2024-T3 induced by acetone degreasing

Devicharan Chidambaram and Gary P. Halada*

Department of Material Science and Engineering, State University of New York at Stony Brook, Stony Brook, NY 11794-2275, USA

Received 22 February 2001; Revised 5 June 2001; Accepted 20 July 2001

Acetone degreasing of aluminum alloy AA2024-T3, as per the ASTM E1078-97 cleaning protocol, showed that copper-rich intermetallic particles acted as a photocatalyst in the presence of moisture to convert the acetone remaining on the surface to acetic acid. In this work, using synchrotron infrared microspectroscopy (SIRMS), we have investigated further the acetone-induced pitting of AA2024-T3 that was shown earlier using XPS. Using SIRMS prior to sodium chloride mist exposure shows the presence of carboxyl groups at sites where pitting is initiated, indicating that pitting is induced by acetone. The infrared linescan and mapping performed on acetone-degreased AA2024-T3 exposed to sodium chloride mist shows the presence of acetyl groups surrounding the pits. Based on this work, acetone is not recommended for degreasing aluminum–copper alloys. Copyright © 2001 John Wiley & Sons, Ltd.

KEYWORDS: acetone; pitting; AA2024-T3; synchrotron; FTIR

INTRODUCTION

Metals, alloys and semiconductors are cleaned using organic solvents such as acetone, isopropanol and methanol, which are considered to be benign. Even the ASTM E1078-97 'Standard Guide for Procedures for Specimen Preparation, Mounting in Surface'¹ recommends that, prior to surface analysis, samples should be degreased ultrasonically in analytical grade acetone and isopropanol. Surface preparation protocols are designed not to alter significantly the surface, otherwise physical or chemical changes could significantly modify the designed performance of a material.

The process of pitting in aluminum alloy AA2024-T3 in aqueous sodium chloride has been the subject of numerous investigations due to the importance of the alloy to aircraft structural engineering.^{2–7} Multiple cleaning and surface preparation processes using organic solvents such as acetone and isopropanol are commonly used in industry.

We have shown previously⁸ that copper acts as a photocatalyst and converts acetone remaining on the surface of copper after degreasing to acetic acid in the presence of ambient water vapor. The acetic acid so formed further attacks copper to form copper acetate, resulting in severe corrosion. This reaction was inhibited completely under dark conditions. In a similar experiment using x-ray photoelectron spectroscopy (XPS), AA2024-T3 was shown to form aluminum acetate when left in ambient laboratory light and atmospheric conditions following exposure to acetone.⁹ However, in a control experiment using commercially pure

aluminum, no such reaction was observed. Therefore, it was proposed that acetic acid was formed in the presence of light on the copper-bearing intermetallic particles in AA2024-T3. This acid was proposed then to have reacted with the surrounding aluminum matrix, producing sufficient acetate to be just detectable by large-area XPS.

In this paper we have investigated further the acetone-induced pitting of AA2024-T3 after exposure to a sodium chloride mist, using synchrotron-based infrared microspectroscopy (SIRMS). This work was performed to confirm the theory proposed earlier⁹ that pitting on exposure to a sodium chloride mist was induced by acetone remaining on the surface of AA2024-T3 after degreasing.

EXPERIMENTAL

Materials and preparation

Commercially anodized AA2024-T3 was obtained as a 3.0 mm thick sheet (Davidson Aluminum & Metal Corporation, New York). The composition of the AA2024-T3 alloy in (wt.%) was 0.5Si, 0.5Fe, 4.42Cu, 0.51Mn, 1.42Mg, 0.09Cr, 0.25Zn and 0.13Ti, with the balance being Al. Acetone and sodium chloride used in this study were ACS grade (J. T. Baker, New Jersey) with a minimum purity of 99.5% and 99.0%, respectively.

Samples were cut into coupons measuring 1 cm², washed with deionized water and ground mechanically with 240-grit SiC paper to remove any surface contaminants. Mechanical polishing was continued with 600-grit and progressively finer grits until a final mirror finish was obtained with a 0.5 µm water-based copper-free alumina suspension (Buehler Ltd, IL; product numbers 40-6375 (1c), 40-6353 (1c) and 40-6377-002). The samples then were rinsed ultrasonically in acetone for 15 min.

*Correspondence to: G. P. Halada, Department of Material Science and Engineering, State University of New York at Stony Brook, Stony Brook, NY 11794-2275, USA.
E-mail: ghalada@ms.cc.sunysb.edu
Contract/grant sponsor: US Air Force Office of Scientific Research; Contract/grant number: F49620-96-1-0479.

Sodium chloride exposure

The 0.5 M NaCl solution was prepared using deionized water. Samples with connecting copper wires were mounted onto Plexiglas™ with a commercial epoxy and attached to a glass rod in a spade-shaped configuration. Ultrahigh-grade dry nitrogen gas was bubbled through a glass frit into the electrolyte for 2.5 h, during which time the sample was held above the electrolyte in the Greene cell. The bubbling of the nitrogen created an aerosol of electrolyte droplets, hereafter referred to as a salt mist, that fell around and on the sample.

Synchrotron infrared microspectroscopy (SIRMS)

The SIRMS technique was performed on samples after ultrasonically degreasing with acetone as well as after exposure to a mist of sodium chloride. A mechanically polished AA2024-T3 specimen was used as the background in these studies.

The SIRMS technique was performed on port U4IR of the vacuum ultraviolet (VUV) ring at the National Synchrotron Light Source (NSLS) of Brookhaven National Laboratory (BNL). The VUV ring (51 m in circumference) was operated at an electron energy of 800 MeV (optimum radiation between 10 eV and 1 keV) and a peak current of 950 mA. The source size was $\sim 1 \text{ mm}^2$ and radiation was emitted into an angle of 90 horizontal by 90 vertical mrad, providing an emittance of $\sim 10^{-4} \text{ mm}^2 \text{ sr}$ (compared with $10^{-2} \text{ mm}^2 \text{ sr}$ for a typical thermal source). The synchrotron provided a 'white' light source ~ 1000 times brighter than a 1200 K thermal source (sometimes called a 'globar'), pulsed at 50 MHz with pulse widths of 500 ps. Light from the synchrotron was collimated and introduced into a commercial Fourier transform infrared (FTIR) microspectrometer (Model IR μ s by Spectra-Tech, Inc., Shelton, CT). The microspectrometer optical train was doubly confocal (i.e. apertures were located before and after the condenser) to limit the interrogated field and to reject the sampling of neighboring surface regions brought about by diffraction. This feature was important when analyzing many adjacent localized regions within a field of view. An aperture size of $10 \times 10 \text{ }\mu\text{m}$ was used for individual spectra and maps. The microscope was used in fixed-focus mode. The regions mapped were chosen to be shallow pits or pits in their initial stages, thereby not compromising the signal-to-noise ratio due to extensive defocusing inside the pits. This was confirmed also from the individual spectrum obtained during mapping from the intensity of the broad water peak centered at ~ 3300 wavenumbers. All spectra were obtained in the reflection mode. Further details of his system and technique have been provided elsewhere.^{10–13} The data were collected with Omnic™ software (Nicolet, USA) and plotted using Microcal Origin™. All wavenumbers used in this study and not specified were obtained from the Spectral Atlas™ database (version 1.0, Academic Press, New York, 1998).

RESULTS AND DISCUSSION

Plate 1(a) shows the optical micrograph of a typical developing pit in an alloy surface washed in acetone. An FTIR mapping was performed on the $100 \times 100 \text{ }\mu\text{m}$

area shown. The IR absorption signal intensity for carboxyl group is shown in Plate 1(b). A typical representative spectrum obtained during the mapping is shown in Plate 1(c). Strong absorption features due to COO^- bond stretching ($\sim 1550 \text{ cm}^{-1}$) and CH_3 bonding ($\sim 1425 \text{ cm}^{-1}$) can be seen clearly in the spectrum. The carboxylate stretching frequency for the acetate group occurs at 1560 cm^{-1} .¹⁴ Aluminum acetate has been shown to have C–O stretching frequencies of $\sim 1595 \text{ cm}^{-1}$ and 1590 cm^{-1} .^{15,16} The carboxyl group stretching for copper acetate is at 1550 cm^{-1} and 1603 cm^{-1} .^{17–19} The alkyl CH_3 deformation occurs at ~ 1430 wavenumbers.¹⁴ The CH_3 deformation for copper acetate occurs at 1456 cm^{-1} ,¹⁹ whereas for sodium acetate it occurs at 1430 cm^{-1} and 1440 cm^{-1} according to two different studies.²⁰ As can be seen, the values identified in this study agree well with the reported values. The mapping for carboxylate bond shows an increasing concentration of the species towards the inside of the pit. The carboxylate bond is specific to acetic acid and hence Plate 1(b) is indicative of the formation of acetic acid from acetone.

Figure 1 shows the optical micrograph of a typical fully developed pit in an alloy surface washed in acetone and then exposed to an NaCl mist. An FTIR linescan was performed on a $150 \text{ }\mu\text{m}$ long path across this region from left to right, as shown. These data are presented in Fig. 2, where the origin of the line is to the left. The data show that the broad hydroxide/bound water peak centered at ~ 3300 wavenumbers shifts slightly to higher frequency as we approach the pit (at about the dark ring shown in Fig. 1), likely indicating a higher force constant related to increased metal coordination. Strong absorption features due to COO^- bonding ($\sim 1550 \text{ cm}^{-1}$) and CH_3 bonding ($\sim 1425 \text{ cm}^{-1}$) also are clearly evident in the region surrounding the pit, both of these being features of acetate or acetyl-acetone groups. Within the pit, these features decrease dramatically and are replaced partly by absorption features in the 500–1000

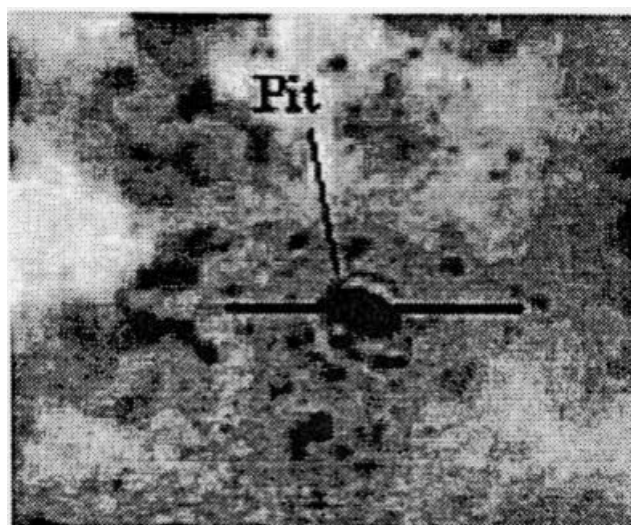


Figure 1. An optical micrograph of AA2024-T3, ultrasonically rinsed in acetone and exposed to sodium chloride mist, showing a typical pit across which an FTIR linescan was performed. The linescan was $150 \text{ }\mu\text{m}$ and was along the line shown above.

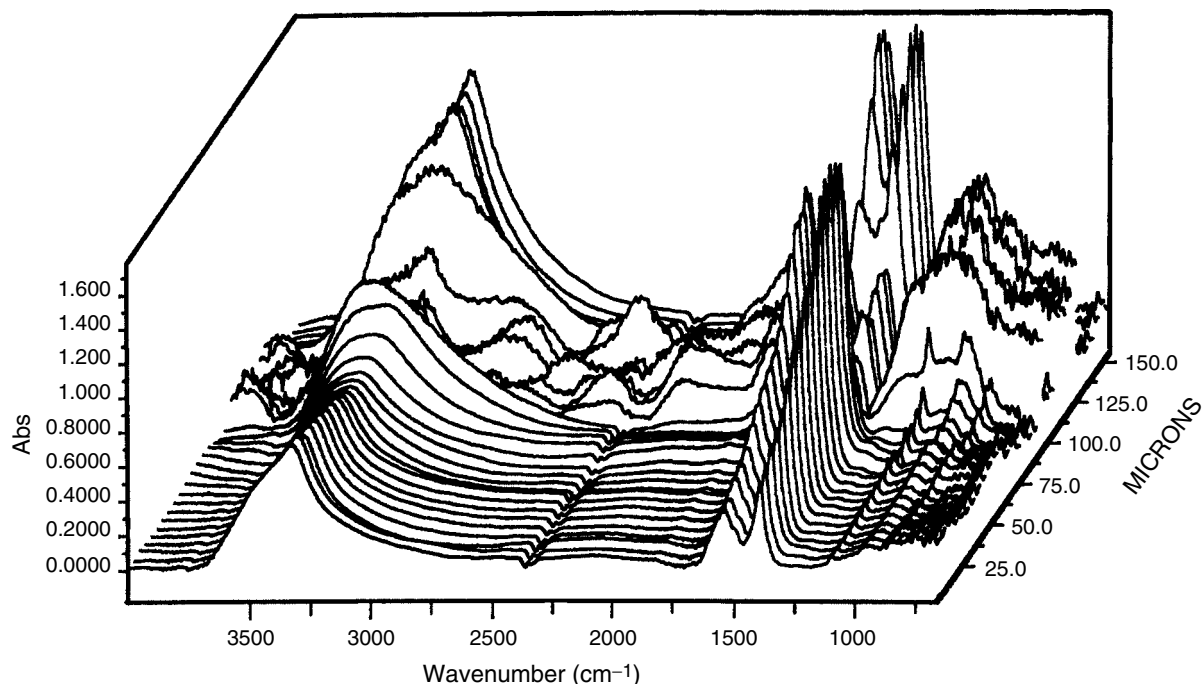


Figure 2. An FTIR line profile across the pit area.

and 1700–2800 wavenumber regions, possibly indicating mixed oxides or metal oxychlorides. It should be noted also that the signal-to-noise ratio as well as the overall signal intensity from the pit were much lower than those from the surrounding area. This is due partially to the low reflectivity from the rough surface of the pit.

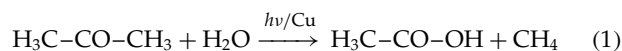
To overcome this difficulty in data collection from a fully developed pit, mapping was performed also at spots that appeared tarnished, indicating the initiation of pitting but not pitted enough to reduce the signal-to-noise ratio significantly. These maps are shown in Plate 2. Plate 2(a) shows the FTIR map of aliphatic hydrocarbon (C–H) bond deformation (1425 wavenumbers) in an area that appeared to have started pitting. It can be seen clearly that the aliphatic carbon is found in high concentrations in the region surrounding the pit. The hydrocarbons could be due to acetone (CH_3COCH_3), acetic acid (CH_3COOH) or acetate (CH_3COO^-) as in copper acetate ($\text{Cu}(\text{CH}_3\text{COO})_2$) and aluminum acetate ($\text{Al}(\text{CH}_3\text{COO})_3$). They could be due also to the sum of all these components.

Plate 2(b) shows the map of a carboxyl group ($\text{O}=\text{C}-\text{O}$) bond stretching in the region ~ 1500 wavenumbers. This could be due to acetic acid (CH_3COOH) or ester as in copper acetate ($\text{Cu}(\text{CH}_3\text{COO})_2$) and aluminum acetate ($\text{Al}(\text{CH}_3\text{COO})_3$). The map indicates that the highest concentrations of the carboxyl groups are at the center of the initiating pit.

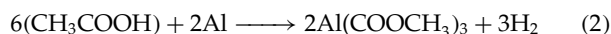
These results suggest that adsorbed acetone on the surface of AA2024-T3 does not induce pitting by itself; rather it is the acetic acid formed on certain locations that induces pitting of the alloy. This leads us to propose that the aliphatic carbon bond stretching shown in Plate 2(a) is likely to be primarily from the acetone (it has two aliphatic carbons) and is high in the region surrounding the pit, whereas the acid or ester is concentrated on the site of pit initiation, as indicated

by the carboxyl group stretching. Hence the acid induces pitting.

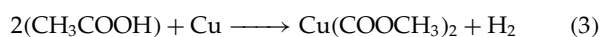
This is consistent with the proposed model of acetone-induced pitting, which is expected to occur on the intermetallic particles containing copper. Various intermetallics such as Al_2Cu , Al_2CuMg , $\text{Al}_2\text{Cu}_2\text{Fe}$, $\text{Al}_7\text{Cu}_2\text{Fe}$, $\text{Al}_{12}\text{Si}(\text{FeMn})_3$, $\text{Al}_{20}\text{Cu}_2(\text{FeMn})_3$ and $\text{Al}_{20}\text{Cu}_3\text{Mn}_3$ are present in AA2024-T3.^{21,22} Both Al_2Cu and Al_2CuMg form two major components among the intermetallic phases in AA2024-T3.^{23–28} Scully *et al.*^{29,30} have shown that the intermetallic surface consisted of CuO in a predominantly Al_2O_3 film and that the CuO created an electrically conducting mixed oxide on the intermetallic surfaces and also enhanced the electron transfer reactions at these sites. The same study also showed that CuO promoted electron tunneling through the aluminum oxide. At these sites, copper acts as a photocatalyst for the reaction between acetone and water. This would be consistent with the formation of acetic acid as proposed earlier⁸ and given below in Eqn. (1)



The acetic acid then reacts with the aluminum in the matrix to form aluminum acetate, as given in Eqn. (2)



Our earlier work showed the aluminum acetate film so formed to be insulating. This film prevents further attack and the aluminum and copper are no longer galvanically coupled. Then the acetic acid reacts with copper⁹ to form copper acetate, as given in Eqn. (3)



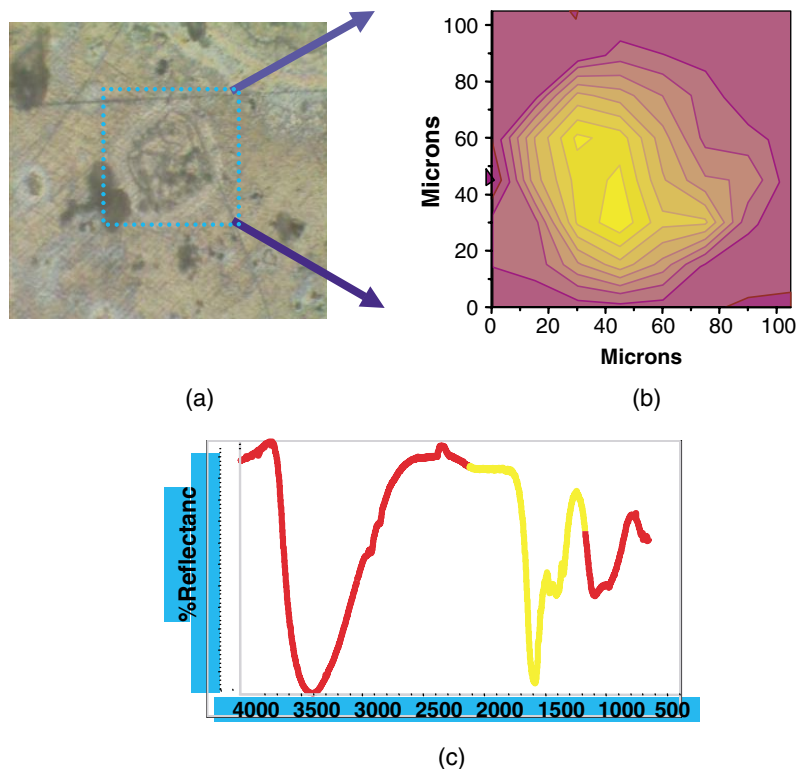


Plate 1. The SIRMS results for an AA2024-T3 sample that had been degreased with acetone prior to exposure to a salt mist in an area that showed initiation of pitting: (a) the dotted-outline box in the optical digimicrograph indicates the region of analysis, which was centred about a site; (b) the SIRMS mapping for carboxyl group bond stretching (1550 cm^{-1}); (c) representative component spectrum emphasizing the spectral region (carboxyl and aliphatic hydrocarbon groups).

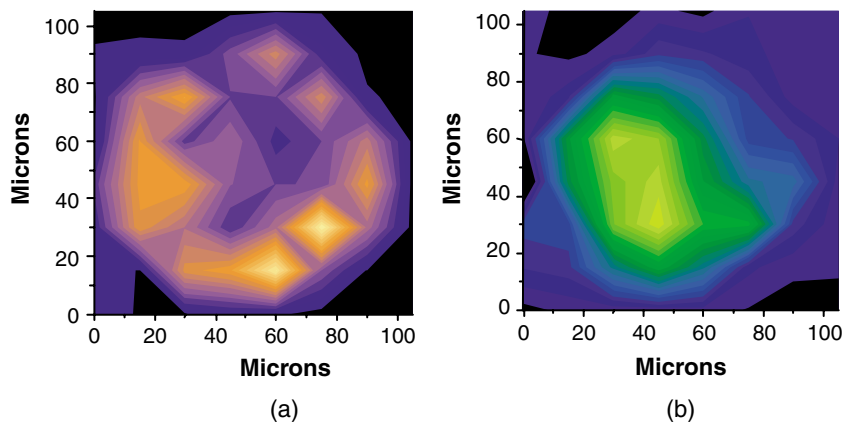
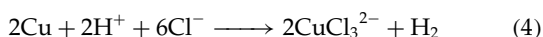
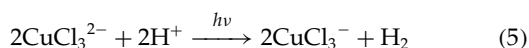


Plate 2. An SIRMS map for: (a) aliphatic hydrocarbon bond deformation (1425 wavenumbers), showing its presence in the region surrounding a site for pit initiation; (b) carboxyl group bond stretching (1550 wavenumbers), showing the presence of acetyl group in the same region. A lighter colour indicates a more intense signal.

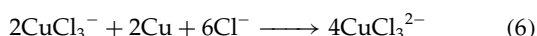
Davis and Johnson³¹(2) suggest the following set of reactions for copper in the presence of acidic chloride solution, as given in Eqn. (4)



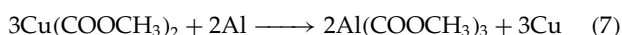
A photooxidation reaction takes place, where the copper complex reacts according to the reaction given in Eqn. (5)



Equation (5) is followed by a self-redox reaction wherein Cu(II) is reduced by copper metal to the more stable Cu(I), as given in Eqn. (6)



Therefore, the aqueous medium along with chloride ions serve to facilitate transport of copper through inducing pitting. The above formation of chlorides in the pitting environment leads to the transport of copper ions out of the pit. Finally, metallic copper is reduced and deposited onto the surface of the ultrathin aluminum passive film. This is given by Eqn. (7)



This behavior is expected from the relative electrochemical activities of aluminum versus the more noble copper under freely corroding conditions that are not highly oxidizing. Hence, as long as the Cu(I) ion deposits on a surface film no thicker than the tunneling distance of electrons, then Cu(I) will be reduced because electrons are liberated by the underlying aluminum oxidizing to Al³⁺. Earlier work⁸ has confirmed the presence of plated copper as observed by optical microscopy.

Aluminum chloride has absorption features at 532.4, 580.5 and 834.4 wavenumbers, copper oxide at 620.6 wavenumbers, and Aluminum oxide at 586.7, 723.7, 636.7 and 820.3 wavenumbers. These form the most intense absorption bands for the compounds. Figure 2 shows that the spectral absorption features in the 500–1000 wavenumber region increase dramatically in the region of the pit. Because sodium chloride has only one absorption band at 454.8 wavenumbers, these observed features may relate to mixed oxides or metal chlorides and thus are consistent with the mechanism proposed by this group for acetone-induced pitting on AA2024-T3.

CONCLUSIONS

Synchrotron infrared microspectroscopy (SIRMS) clearly shows the role that acetone plays in accelerated pitting in copper-containing aluminum alloys such as AA2024-T3. The mechanism proposed earlier by this group—that exposure of AA2024-T3 to acetone in the presence of ambient light and water vapor with chlorides leads to pitting corrosion, with aluminum acetate, metallic copper and copper chlorides, being the primary corrosion products—is supported by this

work. Although the ASTM E1078-97 'Standard Guide for Procedures for Specimen Preparation, Mounting in Surface' recommends that prior to surface analysis the samples should be degreased ultrasonically in analytical-grade acetone and isopropanol, based on our work acetone is not recommended to be used for degreasing aluminum–copper alloys.

Acknowledgements

We acknowledge the National Synchrotron Light Source (NSLS) of the Brookhaven National Laboratory (BNL) for allowing us to use the facilities of the U4IR beamline of the VUV ring. This work was supported by the US Air Force Office of Scientific Research under contract number F49620-96-1-0479. Lt. Col. Paul Trulove, Ph.D., served as the contract officer.

REFERENCES

1. ASTM. *Annual Book of ASTM Standards*, vol. 3.06. ASTM: Philadelphia, PA, 1997; 984–992.
2. Berrada S, Elboujdaini M, Ghali E. *J. Appl. Electrochem.* 1992; **22**: 1065.
3. Mierisch AM, Yuan J, Kelly RG, Taylor SR. *J. Electrochem. Soc.* 1999; **146**: 4449.
4. Sehgal A, Frankel GS, Zoofan B, Rokhlin S. *J. Electrochem. Soc.* 2000; **147**: 140.
5. Zhang WL, Frankel GS. *Electrochem. Solid State Lett.* 2000; **3**: 268.
6. Frantziskonis GN, Simon LB, Woo J, Matikas TE. *Eur. J. Mech. A* 2000; **19**: 309.
7. Li D, Hu YL, Guo BL. *Mater. Sci. Eng. A* 2000; **280**: 173.
8. Kagwade SV, Clayton CR, Chidambaram D, Halada GP. *Electrochim. Acta* 2001; **46**: 2337.
9. Kagwade SV, Clayton CR, Chidambaram D, Du ML, Chiang FP. *J. Electrochem. Soc.* 2000; **147**: 4125.
10. Williams GP. *Rev. Sci. Instrum.* 1992; **63**: 1535.
11. Reffner JA, Martoglio PA, Williams GP. *Rev. Sci. Instrum.* 1995; **66**: 1298.
12. Carr GL, Reffner JA, Williams GP. *Rev. Sci. Instrum.* 1995; **66**: 1490.
13. Dumas P, Carr GL, Williams GP. *Analisis* 2000; **28**: 68.
14. Nakamoto K. *Infrared and Raman Spectra of Inorganic and Coordination Compounds*. John Wiley: Chichester, 1986.
15. Grigorev AI, Maksimov VN. *Russ. J. Inorg. Chem.* 1964; **9**: 580.
16. Alcock NW, Tracy VM, Waddington TC. *J. Chem. Soc. Dalton Trans.* 1976; 2243.
17. Jimenez-Lopez A, Rodriguez-Castellon E, Olivera-Pastor P, Mairele-Storres P, Tomlinson AAG, Jones DJ, Roziere J. *J. Mater. Chem.* 1993; **3**: 303.
18. Masciocchi N, Corradi E, Sironi A, Moretti G, Minelli G, Porta P. *J. Solid State Chem.* 1997; **131**: 252.
19. Chavan S, Srinivas D, Ratnasamy P. *J. Catal.* 2000; **192**: 286.
20. Mehrotra RC, Bohra R. *Metal carboxylates*. Academic Press: New York, 1983.
21. Halada GP, Kearns JR, Vasquez MJ, Clayton CR, Jeanjaquet S, Kendig MW. *193rd Electrochemical Society Meeting*, San Diego, CA, 1998; Abstract 133.
22. Ilevbare GO, Yuan J, Kelly RG, Scully JR. *193rd Electrochemical Society Meeting*, 1998; Abstract 111.
23. Chen GS, Gao M, Wei RP. *Corrosion* 1996; **52**: 8.
24. Gao M, Feng CR, Wei RP. *Metall. Mater. Trans. A* 1998; **29**: 1145.
25. Wei RP, Liao CM, Gao M. *Metall. Mater. Trans. A* 1998; **29**: 1153.
26. Pires I, Quintino L, Rangel CM, Thompson GE, Skeldon P, Zhou X. *Trans. Inst. Met. Fin.* 2000; **78**: 179.
27. Buchheit RG. *Mater. Sci. Forum.* 2000; **331–333**: 1641.
28. Obispo HM, Murr LE, Arrowood RM, Trillo EA. *J. Mater. Sci.* 2000; **35**: 3479.
29. Scully JR, Peebles DE, Romig AD, Frear DR, Hills CR. *Metall. Trans. A* 1992; **23A**: 2641.
30. Scully JR, Knight TO, Buchheit RG, Peebles DE. *Corros. Sci.* 1993; **35**: 185.
31. Davis DD, Johnson DL. *J. Electrochem. Soc.* 1978; **125**: 1889.